Title
Photolytic Processing of Organic Aerosol through Carbonyl Photochemistry

Author
Blair, Sandra Louise

Publication Date
2014

Peer reviewed|Thesis/dissertation

UNIVERSITY OF CALIFORNIA,
IRVINE

Photolytic Processing of Organic Aerosol through Carbonyl Photochemistry

THESIS

submitted in partial satisfaction of the requirements
for the degree of

MASTER OF SCIENCE

in Chemical and Materials Physics-Chemistry

by

Sandra Louise Blair

Thesis Committee:
Professor Sergey Nizkorodov, Chair
Professor Barbara Finlayson-Pitts
Assistant Professor Craig Murray

2014

DEDICATION

To

My Mom, Donna Blair, my rock.

My Gramps, Richard Blair, the person who always believed in me, and who offered me his kitchen for my first experiments. I wish you were here today so I could show you all that I have learned.

I also dedicate this to

The Chemistry Department at California State University Chico for becoming a second family to me. You provided me with many job and research opportunities to financially support myself and to grow as a chemist. In particular, Professor Randy Miller introduced me to Physical Chemistry and had an enthusiasm for teaching with a lasting effect.

TABLE OF CONTENTS

LIST OF SYMBOLS

Symbol	Definition	Unit
$\sigma(\lambda)$	Base e Absorption Cross Section	$\frac{cm^2}{molecule}$
$\phi(\lambda)$	Quantum Yield	$\frac{molecules}{photon}$
$D_o(\lambda)$	Spectral Flux Density of Radiation	$\frac{photons}{cm^2 \cdot s \cdot nm}$
M_{ppbv}	Gas-Phase Concentration of PTR-ToF-MS Analyte	ppb
ρ	PTR-ToF-MS Proportionality Constant	ppb
T_{drift}	Drift Temperature	K
T_o	Temperature at Standard Condition	K
p_o	Pressure at Standard Condition	mbar
p_{drift}	Drift Pressure	mbar
$[MH^+]$	PTR-ToF-MS Parent m/z Analyte Signal	cps
$[H_3O^+]$	PTR-ToF-MS Hydronium ion m/z Signal	cps
$TR_{(H_3O^+)}$	Transmission Efficiency of Hydronium ion	N/A
$TR_{(MH^+)}$	Transmission Efficiency of Analyte Ion	N/A
$r(MH^+)$	Isotopic Ratio of Parent Analyte Ion	N/A
μ_0	Reduced Mobility	$\frac{cm^2}{V \cdot s}$
$k_{H_3O^+}$	Reaction Rate Constant for Analyte with Hydronium ion	$\frac{cm^3}{s \cdot molecule}$
l	Drift Tube Length	cm
U_{drift}	Drift Voltage	V
$\mathcal{J}$	Photolysis Rate Constant	s^{-1}
R	Photolysis Rate	$\frac{molcules}{cm^2 \cdot s}$

$f_{irradiated}$	Fraction of Sample Irradiated	N/A
b	Pathlength of Cell	cm
n	Number Concentration of Analyte	$\frac{molecules}{cm^3}$
$OO(\lambda)$	Ocean Optics Output	N/A
α	Proportionality Constant	$\frac{photons}{cm^2 s}$

LIST OF FIGURES

LIST OF EQUATIONS

LIST OF TABLES

ACKNOWLEDGMENTS

I am extremely grateful to my committee chair, Professor Sergey Nizkorodov, for invaluable guidance in my graduate career, supporting my "Rosie the Riveter" approach to research, patience in listening to my exponentially increasing line of thinking, and whose excitement for chemistry and teaching is very contagious.

I would like to thank my committee members, Professor Barbara Finlayson-Pitts and Assistant Professor Craig Murray, for their support and suggestions throughout the research and writing of this thesis.

Financial support was provided by the University of California, Irvine, NSF Grant AGS-1227579**,** and NSF Grant CHE-0909227**.**

ABSTRACT OF THE THESIS

Photolytic Processing of Organic Aerosol through Carbonyl Photochemistry

By

Sandra Louise Blair

Master of Science in Chemistry and Materials Physics-Chemistry

University of California, Irvine, 2014

Professor Sergey Nizkorodov, Chair

Atmospheric aerosol is known to have a direct effect on the radiative forcing of the climate by absorbing and scattering light and an indirect effect by acting as cloud condensation nuclei. Organic aerosol (OA), sometimes the major contributor to atmospheric aerosol, contains highly oxidized, multifunctional, low vapor pressure organic compounds. Carbonyls play a significant role in the photochemistry of secondary organic aerosol (SOA) as the near-UV absorption spectra of SOA are dominated by the C=O $\pi^* \leftarrow n$ transition. SOA photochemistry can be expected to be driven in part by the well known photochemical reactions of carbonyls such as Norrish and Yang mechanisms. Therefore, investigating a model carbonyl, such as a linear chain aldehyde, in an environment that mimics SOA should provide valuable information on the mechanism and rate of photochemical processes occurring in SOA. The pure form of an aldehyde will act as its own SOA-like organic matrix. The quantum yield of photolysis may be suppressed in the condensed-phase, but might still be significantly high to make photolysis relevant. A C_{11} aldehyde, undecanal, is investigated in this thesis as a model for this carbonyl photochemistry in OA. Undecanal photolysis was investigated at room temperature in

liquid and gas phases. Products were analyzed with gas chromatography mass spectrometry or proton transfer reaction mass spectrometry. The products, quantum yields, and rate constants of undecanal in each environment were compared. Results suggest that the loss of carbonyls due to photolysis in the condensed-phase should be just as important as the photochemistry in the gas-phase.

INTRODUCTION

Air pollution from particulate matter (PM) and gases have harmful effects on health, climate, and visibility.[1] The six regulated criteria pollutants are PM, ozone, carbon monoxide (CO), nitrogen oxides, sulfur dioxide, and lead. PM is known to have negative cardiovascular, respiratory, morbidity, and mortality effects and is suggested to also cause reproductive and developmental problems, impaired cognitive abilities, and cancer.[2, 3] Recent studies have shown the occurrence of these health effects at even lower ambient concentrations than previous studies.[2] The World Health Organization estimated that 3.7 million deaths globally were attributed to PM with a diameter of 10 μm and less (PM_{10}) from ambient air pollution of 2012.[4] Fresno and Madera, California, became the most polluted cities in the nation for short-term and year-round particle pollution for data covered from 2010-2012.[5] PM contains many different compounds including sulfates, nitrates, organics, ammonium, and chlorides.[6] Organic aerosol (OA) is significant and sometimes the major component of $PM_{2.5}$ and PM_{10},[7-9] providing 20-90% of the submicron particle mass.[6-9] OA ages in heterogeneous processes such as oxidation by radicals (OH[10] and NO_3[11]) and molecular O_3,[12] acid catalyzed oligomer formation[13] and cyclization,[14, 15] and photolysis.[10, 16] In addition to health effects, particles can affect the climate directly by absorbing or reflecting solar light and indirectly by acting as cloud condensation nuclei, and can dramatically reduce visibility.[17]

In the atmosphere, the presence of oxygen filters out the vacuum UV ($\lambda < 200$ nm) and the ozone layer absorbs hard UV ($200 \text{ nm} < \lambda < 300$ nm) radiation, allowing photochemistry of labile chromophores in aerosol within the actinic region ($\lambda > 300$ nm).

Secondary organic aerosol (SOA) functional groups that are photolabile within the actinic region include carbonyls, nitrates, peroxides, and a variety of conjugated systems. This research looks specifically at the carbonyl, contributing to an average of approximately 23%[18-21] of SOA functional groups. Carbonyls play a significant role in the photochemistry of SOA as the absorption spectra strongly correspond to the C=O $\pi^* \leftarrow n$ transition around 290 nm.[22] SOA photochemistry can be expected to be driven in part by the well known photochemical reactions of carbonyls such as Norrish[23] and Yang[24] mechanisms. Therefore, investigating model carbonyls, such as linear chain aldehydes, in an environment that mimics OA should provide valuable information on the mechanism and rate of photochemical processes occurring in SOA.

Most previous photochemical studies of saturated linear chain aldehydes were done in the gas-phase.[25] In contrast, the importance of photochemistry occurring in condensed phases in the atmosphere has not been recognized until recently.[26-29] Our understanding of particle photochemistry is only qualitative at this point as few studies have been conducted using an organic matrix of the type one could encounter in OA.[16, 22] There are many organic matrices that could mimic the environment found inside an SOA particle. Our approach is to use the pure form of an aldehyde that will act as its own organic matrix. A C_{11} aldehyde, undecanal, provides a model for this carbonyl photochemistry. Its vapor pressure is high enough such that it provides access to different states (solid, liquid, gas) in a convenient temperature range. Undecanal photolysis was investigated at room temperature in liquid and gas-phases. The products, rate constants, and quantum yields of undecanal in each environment were compared. The goal of this research is to probe the importance of aldehyde photochemistry in SOA compared to its gas-phase.

CHAPTER 1: Literature Survey

Norrish[23] and Yang[24] mechanisms are well known in the photochemistry of carbonyls and similar products can be expected to form in the photolysis of undecanal as seen in Figure 1.1. Carbonyls of aliphatic aldehydes exhibit a weak absorption band between 240-360 nm for an $\pi^* \leftarrow n$ transition to form an excited 1,2-biradical (BR1).[30, 31] The Norrish Type I radical process involves α-cleavage to give both an alkyl (A1) and acyl (A2) radical. A subsequent hydrogen transfer from A2 to A1 produces molecular products including an alkane and carbon monoxide. Photochemical aldehydic-hydrogen detachment is also possible, but very minor.[30, 32] If the excited BR1 has a carbon chain length, C_n, of at least n=4 and has a geometry such that it can form a six-membered ring, a gamma hydrogen may be transferred to the oxygen forming a 1,4-biradical (BR2) in the Norrish Type II reaction.[33] Delta hydrogen transfers are also possible, but are less likely (~5%), especially with non-substituted alpha carbons of linear aldehydes.[34] The H-transfer is followed by a beta cleavage of the BR2 to yield an alkene and vinyl alcohol which quickly tautomerizes[35] to acetaldehyde. Yang Photocyclization of the BR2 leads to an alkyl cyclobutanol; this is generally a minor product compared to Norrish Type I alpha cleavage and Norrish Type II beta cleavage.[24, 36]

The photochemical pathways of linear saturated aldehydes depend on chain length and surrounding environment. The Norrish Type II channel opens up as an aldehyde chain reaches four carbons in length, providing a γ-H for intramolecular abstraction.[33] Going from a C_4 to a C_5 linear saturated aldehyde, the Norrish Type II pathway increases due to

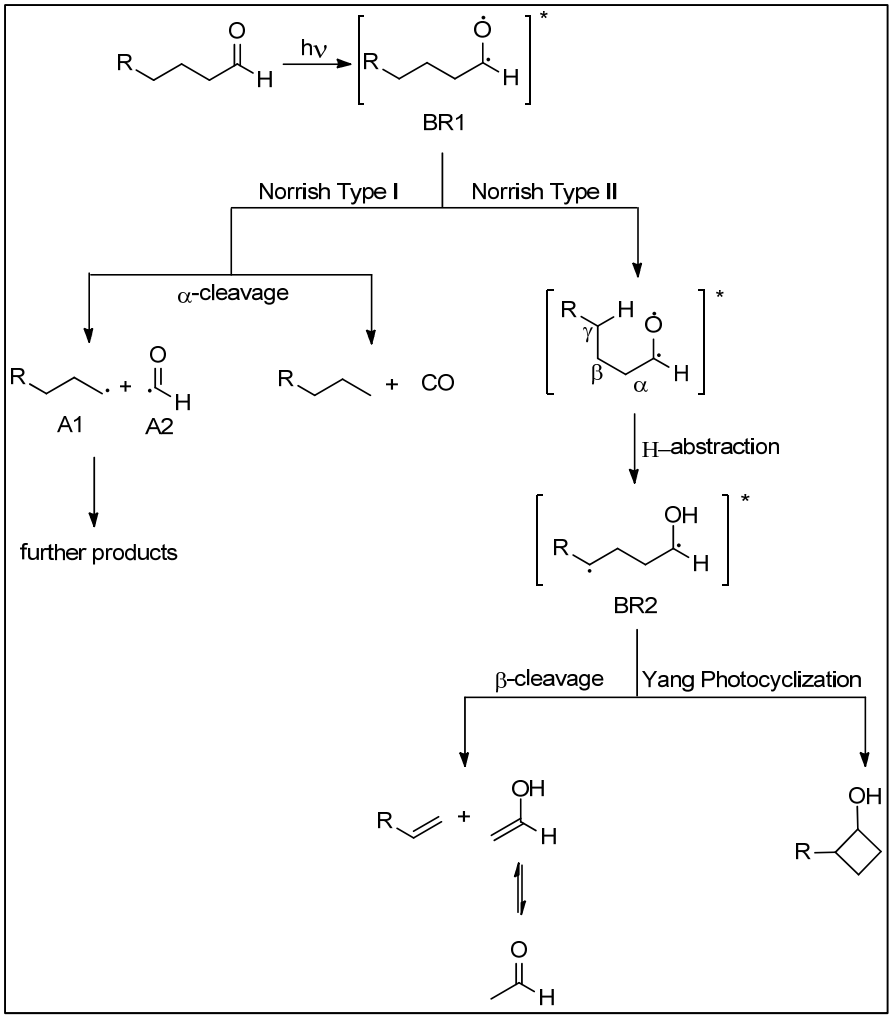

Figure 1.1 Pathways of aldehyde photolysis[23,24]

the availability of a secondary γ-H (versus a primary of the C_4 species); larger chain aldehydes have similar yields as a C5 aldehyde.[37] When this is possible and BR2 is formed, it may convert back to the starting aldehyde via disproportionation.[38] The surrounding environment may vary between solvent type, phase, and temperature. It plays a large role in the evolution of radical species. In the gas-phase, photochemically produced radicals will react with molecules and radicals in the air and most likely result in alkoxy radicals that can then either lead to oxidation, isomerization, or decomposition products.[26] In comparison, condensed-phase photochemistry offers an environment with many more

possible complex reaction mechanisms. Solvents can affect the energy difference between the $\pi^* \leftarrow n$ and $\pi^* \leftarrow \pi$ transitions where the latter might have a lower excitation energy and decrease the photolysis quantum yield in polar solvents.[38] Condensed media may also add a "cage effect" where reactions are diffusion limited.[39] The magnitude of this effect depends on the solvent viscosity. If the radicals react faster than they can diffuse through the solvent then a "solvent cage" is formed where the radicals recombine or disproportionate inside the cage. The condensed environment can also limit the ability for rotation to favorable geometries. A basic solvent may inhibit the BR2 disproportionation to the starting aldehyde by stabilization of the hydroxyl group with hydrogen bonding.[38] More viscous solvents and colder temperature conditions can prevent BR1 from forming BR2 thus decreasing the Norrish Type II and Yang photocyclization products due to geometry restrictions. A temperature difference of 10 °C can reduce the photolysis rate constant by a factor of 2-4.[40]

In the family of saturated linear chain aldehydes, formaldehyde, acetaldehyde, and propanal have been studied the most frequently.[25, 41-43] There are some photochemical studies of C_4-C_7[37, 44-48] aldehydes and few studies of C_8[36] and longer aldehydes[49, 50], which are more relevant for the condensed-phase atmospheric photochemistry. Aqueous[51], organic solvent,[52] polymer,[53] solid,[54] and surface[55] photochemical studies of aldehydes exist, but SOA-like organic matrix-phase studies are rare.[38] This more atmospherically relevant SOA-like phase in aldehyde photochemistry is investigated.

CHAPTER 2: Experimental Methods

I. Gas-Phase Photochemistry

All experiments were done at 1 atm. The experimental setup consists of a 300 L Teflon chamber coupled to an Ionicon reflectron Proton Transfer Reaction-Time of Flight-Mass Spectrometer (PTR-ToF-MS). The chamber is equipped with 16 UV lamps (Philips 40W Ultraviolet B TL 40W/12 RS SLV), an injecting port, and a sampling valve to the PTR-MS. The PTR-ToF-MS offers real time photochemical analysis of species with high resolution. Gaseous molecules with proton affinities greater than that of water (165 kcal/mol)[56] are ionized by H^+-transfer and can be detected. Acetone actinometry was used to calculate the spectral flux density of the lamps (see Figure 2.1). Actinometry experiments were done separately from undecanal photolysis. The photolysis rate constant and quantum yield calculations for actinometry and undecanal are seen in the Appendix (for both gas- and condensed-phase experiments). Acetone photolysis quantum yields and absorption cross section data were taken from JPL.[25] Hexanal absorption cross section data from the MPI-Mainz-UV-VIS Spectral Atlas[57] was used to model that of undecanal; the absorption cross sections of C_4 and larger linear saturated aldehydes are practically identical.[36]

Solutions of each analyte (~0.40 M) were prepared in methylene chloride so that concentrations in the ppbv range were possible to attain. Methylene chloride does not absorb light in the region that the lamps radiate and its photolysis is negligible.[58] The Teflon bag was partially filled with zero air, a few microliters of solution were injected through the septum, and the bag was filled with more zero air. Calibration experiments

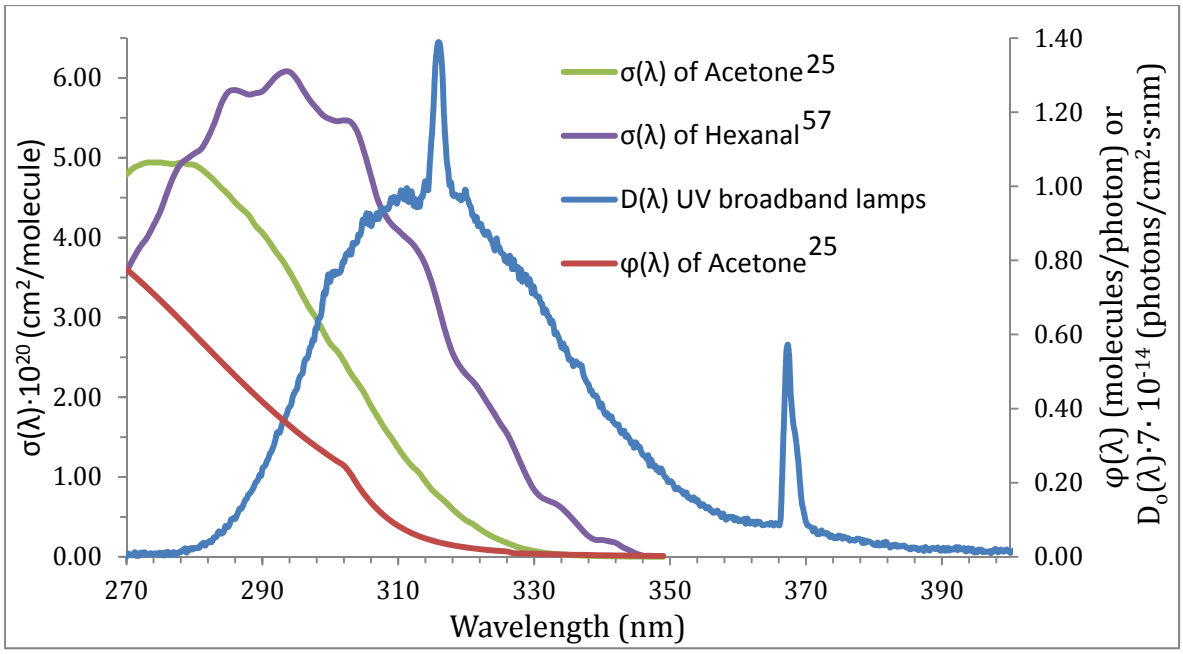

Figure 2.1 Gas-phase actinometry data. Gas-phase spectral flux density, $D_o(\lambda)$; absorption cross sections, $\sigma(\lambda)$; and quantum yield, $\phi(\lambda)$. Acetone data was taken from JPL[25]; hexanal data was from the MPI-Mainz-UV-VIS Spectral Atlas[57].

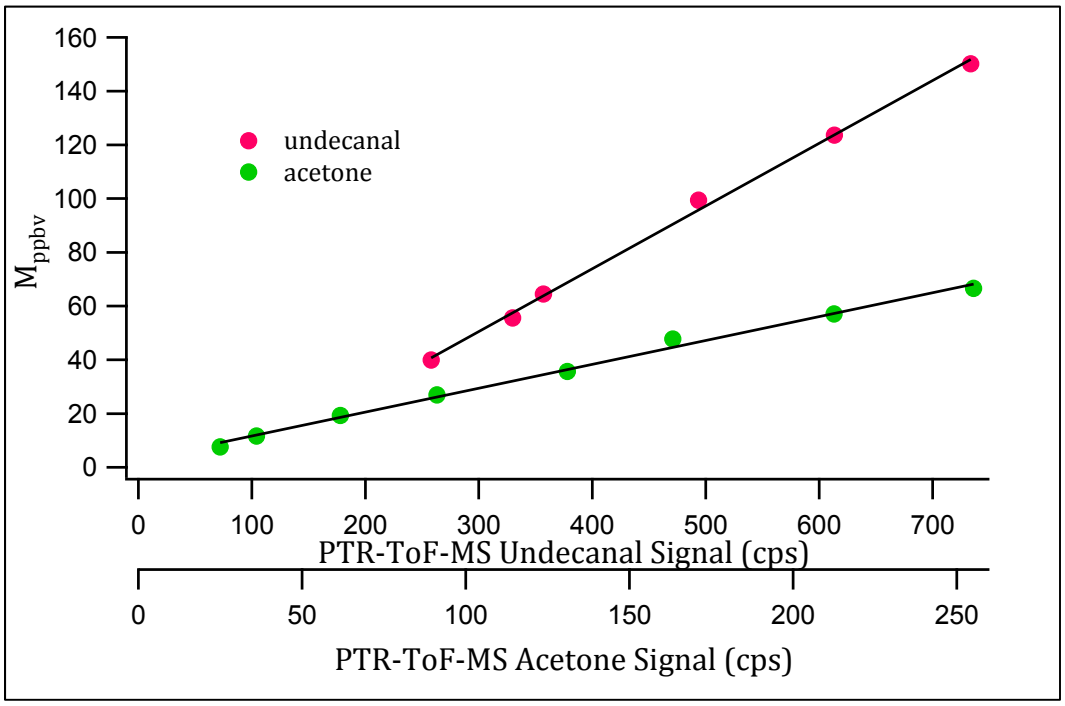

Figure 2.2 PTR-ToF-MS calibration of acetone and undecanal.

were conducted for each analyte of known concentration (see Figure 2.2). Several concentrations and corresponding signals of the analyte were measured by dilutions with zero air in calibration experiments; signals were normalized by temperature, pressure, and hydronium ion concentration as seen in Equation 2.1. The first term, ρ, is a proportionality constant. It does not change between experiments of the same analyte. Therefore, transmission ratios and proton transfer reaction rate constants were not required and ρ was extracted by a linear fit. The drift voltage (U_{drift}), temperature (T_{drift}), and pressure (p_{drift}) were 600 V, 60 °C, and 2.35 mbar. The drift tube length (l) and reduced mobility (μ_0) are 9.3 cm and 2.8 $cm^2 \cdot V^{-1} \cdot s^{-1}$. After the analyte signal stabilized, the lamps were turned on and photolysis was allowed to proceed for ~4 hours. The wall loss was negligible in both cases, as established in radiation-free runs. The acetone and undecanal parent peaks, [MH^+], were monitored at *m/z* 59.0497 and *m/z* 171.1749. The time evolution of various peaks in the mass spectrum were monitored. Experiments were done in duplicate.

$$M_{ppbv} = \boldsymbol{\rho} \cdot \frac{T_{drift}^2(K)}{T_o^2(K)} \cdot \frac{p_0^2(mbar)}{p_{drift}^2(mbar)} \cdot \frac{[MH^+]}{[H_3O^+]}$$

$$\boldsymbol{\rho} = \frac{TR_{(H_3O^+)} \cdot 10^9 \cdot 22400 \cdot \mu_0}{r(MH^+) \cdot TR_{(MH^+)} \cdot k_{H_3O^+} \cdot N_A \cdot l^2} \cdot U_{drift}$$

Equation 2.1 PTR-ToF-MS calculations. Concentration of analyte, M_{ppbv}, in ppbv predicted from the experimental parameters for the PTR-MS instrument. See text for the definition of different terms.

II. Condensed-Phase Photochemistry

A temperature-controlled sample cell with 1 inch diameter calcium fluoride windows and an adjustable pathlength from Harrick Scientific (TFC-M25-3) was used in these experiments. Light traveled from a xenon arc lamp (Newport model 60100) through a 295 nm long pass filter and a focusing lens to the sample cell. The Teflon spacer path length was calculated from transition interference fringes appearing in the FTIR spectrum (Mattson Galaxy 5030), and was 920 μm. An actinometer, 2-nitrobenzaldehyde (2NBA), in a methylene chloride solution, was monitored at its FTIR -NO_2 symmetric vibration[59] at 1348 cm^{-1} as seen in Figure 2.3 (calibration experiments of 2NBA were conducted as well). Photolysis converts 2NBA to its isomeric form with a wavelength independent quantum yield of 0.5,[60-62] and this process can be monitored by FTIR with a decrease in the 1348 cm^{-1} peak. The 2NBA photolysis rate constant, $\mathcal{J}_{2NBA}(s^{-1})$, was $(2.17 \pm 0.30) \cdot 10^{-2}$. The spectral flux density and absorption cross sections are seen in Figure 2.4. Undecanal was photolyzed in its pure liquid form where it acted as its own organic matrix. Following photolysis, the samples were diluted in methylene chloride ($\sim 10^{-4}$ M) and were analyzed with a Thermo Trace electron impact gas chromatography mass spectrometer (GCMS) for decane standard addition experiments. Undecane was used as an internal standard.

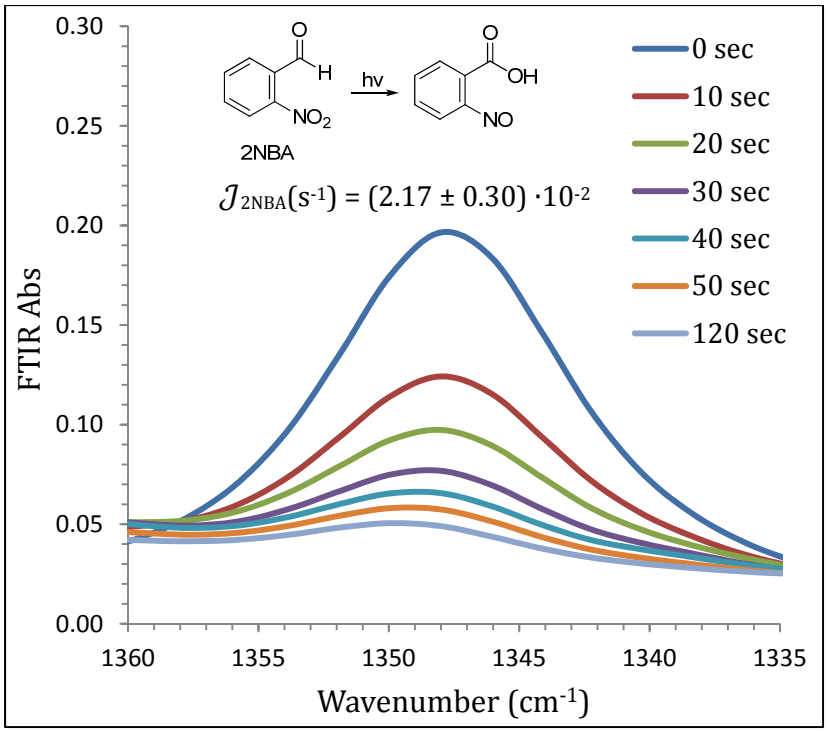

Figure 2.3 2NBA actinometry.

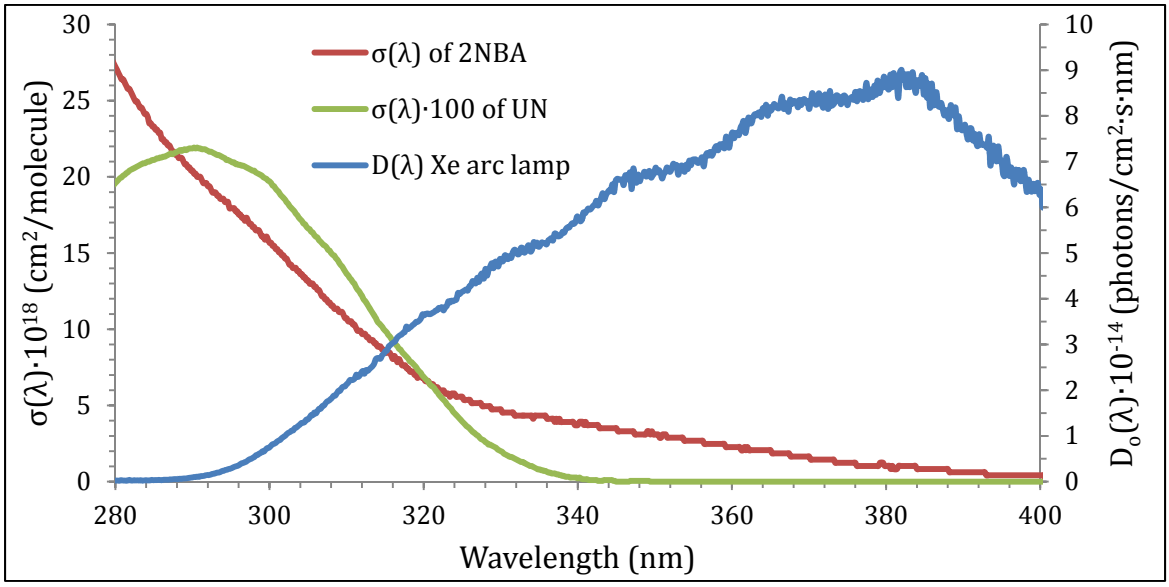

Figure 2.4 Condensed-phase absorption data. Spectral flux density with a 295 nm long pass filter, $D_o(\lambda)$; and absorption cross sections, $\sigma(\lambda)$.

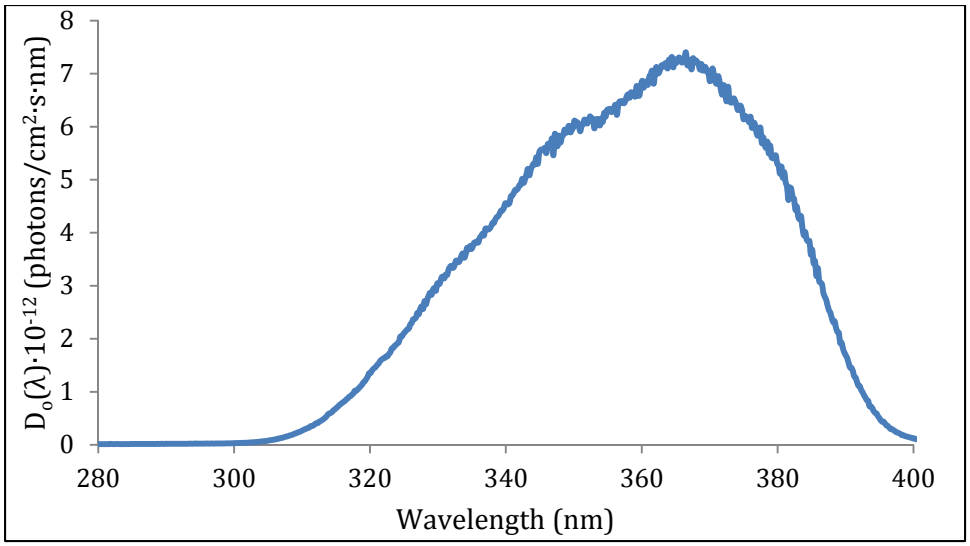

Figure 2.5 Condensed-phase absorption data 2. Spectral flux density with a 360 nm band pass filter, $D_o(\lambda)$.

A second set of experiments was performed with a similar setup as previously described except that the 295 nm longpass filter was replaced with a 360 bandpass filter. This created a photolysis spectral flux density to better mimic that of the gas-phase experiments (see Figure 2.5). FTIR spectroscopy was used to investigate product formation for the spectral flux density seen in Figure 2.5.

CHAPTER 3: Results and Discussion

I. Gas-Phase Photochemistry

First order rate constants, $\mathcal{J}_{AC}(s^{-1})$ and $\mathcal{J}_{UN}(s^{-1})$, are extracted from PTR-ToF-MS photolysis data for acetone, $(1.13 \pm 0.03)\cdot10^{-5}$, and undecanal, $(4.77\pm 0.14)\cdot10^{-5}$, in Figure 3.1. Undecanal has larger absorption cross sections than acetone and has a wavelength of maximum absorption near 290 nm (acetone: 275 nm) which has better overlap with the lamp emission than acetone. This allows undecanal to photolyze ~4 times faster than acetone. Table 3.1 shows quantum yields from these experimental results along with literature values[36] of other linear saturated aldehydes.

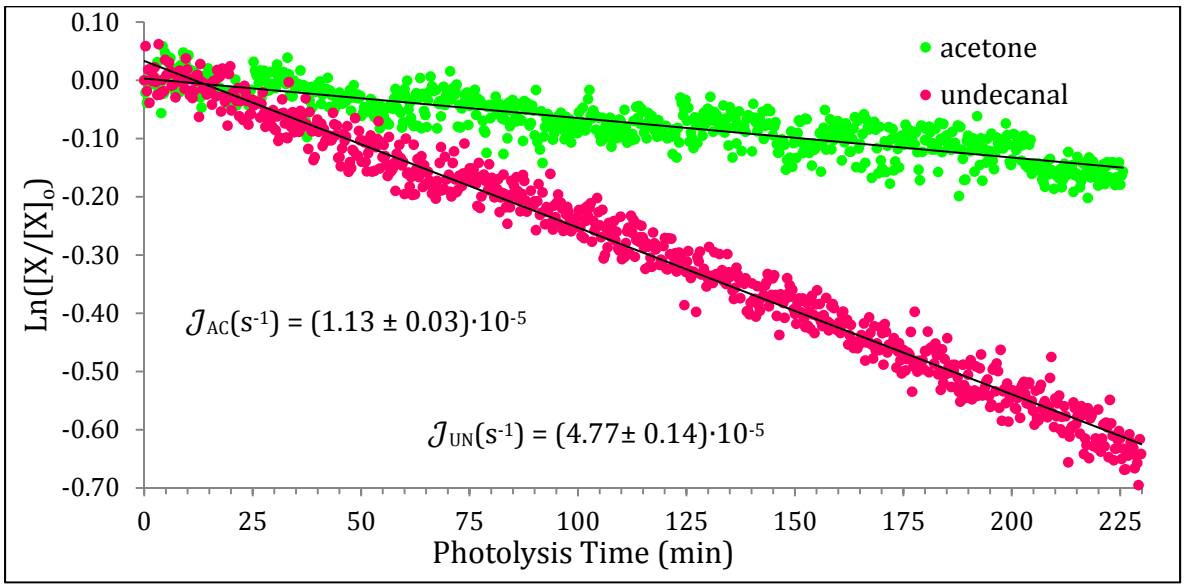

Figure 3.1 Gas-Phase Acetone and Undecanal Photolysis (Separate experiments; X = analyte). The photolysis rate constants were calculated from the slopes of the lines.

Table 3.1 Gas-phase Quantum Yields of Linear Saturated Aldehydes. Literature values of C4-C7 are from Tadic et al[36].

Aldehyde	**ϕ**	**Notes**
C_4	0.32 ± 0.02	Appearance of Norrish Type I and II products monitored at 700 Torr by Tadic et al[36]
C_5	0.34 ± 0.02	
C_6	0.38 ± 0.02	
C_7	0.31 ± 0.01	
C_8	0.32 ± 0.01	
C_{11}	**0.29 ± 0.11**	**Loss of undecanal at 760 Torr**

Undecanal parent ions underwent water loss and further fragmentation with peaks at *m/z* values (and intensities normalized to the largest peak) of 83 (100%), 171 (20%), 97 (8%), 69 (4%), 153 (2%), and 111(2%). The m/z peak at 153 was from water loss and the rest of the peaks are alkyl chain fragments. The parent 171 peak was monitored as it was unique from any expected product fragments. Figure 3.2 shows the signals in relative counts per second (cps) of undecanal and a few identified photoproducts. There is a very large increase in the Norrish Type II product, acetaldehyde, with photolysis time. From this result the co-photoproduct, 1-nonene, would also be expected to form, but its parent peak was not detected in the mass spectrum. PTR-ToF-MS data of a 1-nonene standard, which could be measured at higher concentrations, showed that it had fragmented significantly, m/z values of 57 (100%), 71 (75%), 85 (36%), and 127 (5%), compared to Diskin et al[63]. The 57 and 71 *m/z* peaks are common for alcohols;[64] this 1-nonene fragment cannot be isolated from other product fragments.

Decanal is also observed to increase, forming from the Norrish Type I mechanism and oxidation of the A1 decyl radical (see Figure 3.3).[65] Peroxidation of the formyl radical (A2), from the Norrish Type I pathway, ultimately leads to formic acid as seen in Figure 3.4.[53, 66, 67] Decane may have formed, but is not detected with PTR-ToF-MS as it is not expected to ionize efficiently as alkanes do not have proton affinities larger than water. Hexane is the largest alkane with a calculated proton affinity of 162 kcal/mol; increasing the chain length by a single carbon increases the proton affinity only by a few kcal/mol.[68] Aldehyde, alcohol, ester, and ketone (somewhat) parent ions are known to further fragment in PTR-ToF-MS.[64] Other possible products could not be identified due to their overlap of common fragment ions.

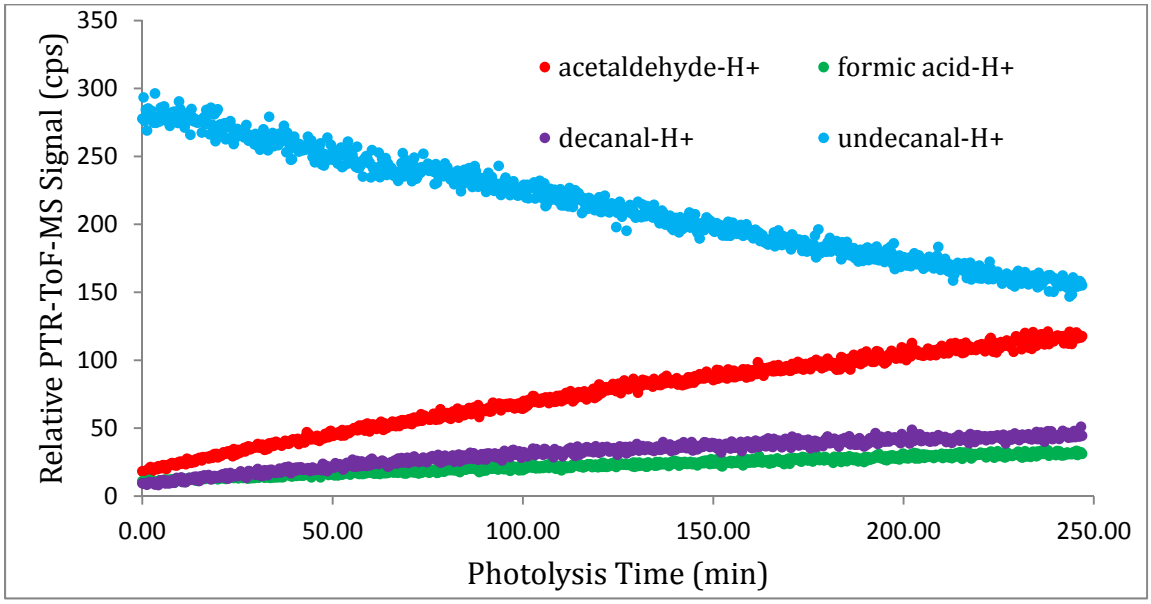

Figure 3.2 PTR-ToF-MS Data of Gas-Phase Undecanal Photolysis.

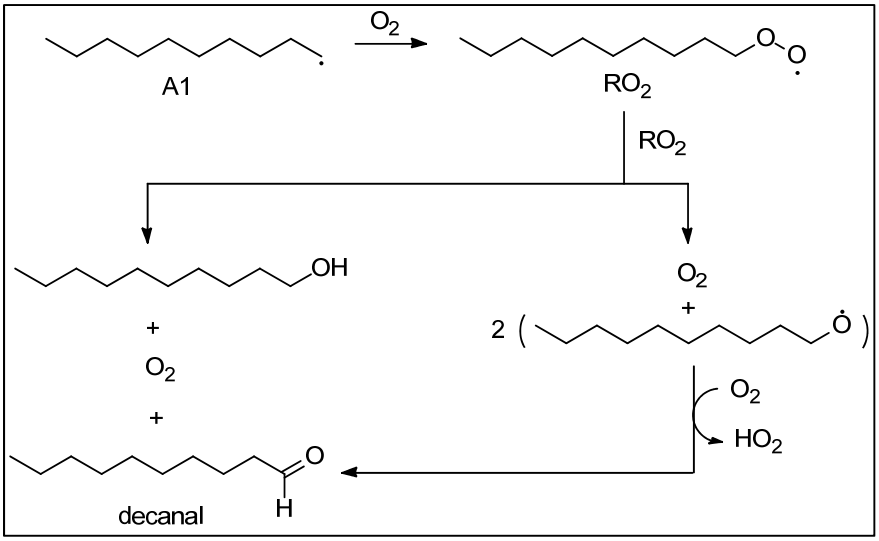

Figure 3.3 Formation of decanal.

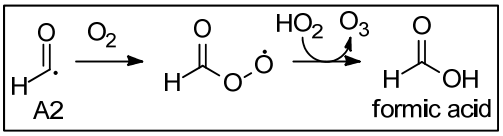

Figure 3.4 Formation of formic acid.

The quantum yield of undecanal determined relative to that of acetone, 0.29 ± 0.11, was similar to linear saturated aldehydes studied by Tadic et al[36]. Note that possible secondary chemistry was not taken into account, but will be modeled in the future where branching ratios of the Norrish Type I and II products can be calculated. Our experiments measured the loss of the starting aldehyde whereas Tadic et al[36] measured the formation of products for the quantum yield calculation. These experiments were also done at a higher pressure; one could expect a smaller quantum yield due to increased collisional induced relaxation of the excited aldehyde, but, within uncertainty, the quantum yields are not different. The photolysis conditions were very similar to these experiments, as wide band emission lamps produced radiation of 275-380 nm.[36] This similar quantum yield results can be expected, as linear saturated aldehydes have practically identical absorption cross sections.[36]

II. Condensed-Phase Photochemistry

The main difference between the gas- and liquid-phase photolysis is that, aside from autoxidation, condensed-phase reactions of free radicals may include facile radical-radical recombination, disproportionation, and intermolecular abstraction.[69-73] Also, a bimolecular autoinhibition mechanism with BR1 and starting material (i.e., undecanal) may occur in the condensed phase (see Figure 3.5).[70] The undecanal photolysis rate constant, J_{UN}(s^{-1}), was calculated from the curve in Figure 3.6 to be $(8.35 \pm 0.35)\cdot 10^{-5}$. A Norrish Type I product, decane, was the only newly formed peak in the GCMS chromatogram. The loss of undecanal was attributed to the formation of decane and, under this assumption, the calculated undecanal photolysis quantum yield is a lower limit. Although decane may directly form from this pathway, the condensed-phase offers neighboring aldehyde molecules as a hydrogen abstraction source for the initially formed Norrish Type I decyl radical.[69-73] For example, Kossanyi et al[69] photolyzed benzophenone in an excess of butanal and proposed that H-abstraction of the aldehyde would occur, and another butanal molecule could H-abstract from the protonated benzophenone radical to give the starting ketone and proceed in a "chain-like" reaction. The benzophenone quantum yield should have been less than 1 if only these two processes occurred, but was 1.4 owing to additional radical reactions. It was explained that the lager quantum yield would arise from cross-molecular reactions of radicals with the ground state benzophenone.[69]

It was assumed that the photolysis rate of undecanal was equivalent to or greater than the rate of formation of decane. The calculated quantum yield was 0.18 ± 0.01 and was based solely on the formation of decane, which is a lower limit. Paquet et al[70] had photolysis quantum yields of pentanal for alpha-dione and alpha-ketol of 55% and 38%

with radiation at 355 nm. The differences in the quantum yields and products may come from the fact that this data reports an average quantum yield over a broad range of wavelengths. There may also be other undetected products of undecanal that are formed that are either hidden within the saturated undecanal chromatogram peak or elute with the solvent. Further experiments that monitor undecanal starting material are required to validate this quantum yield.

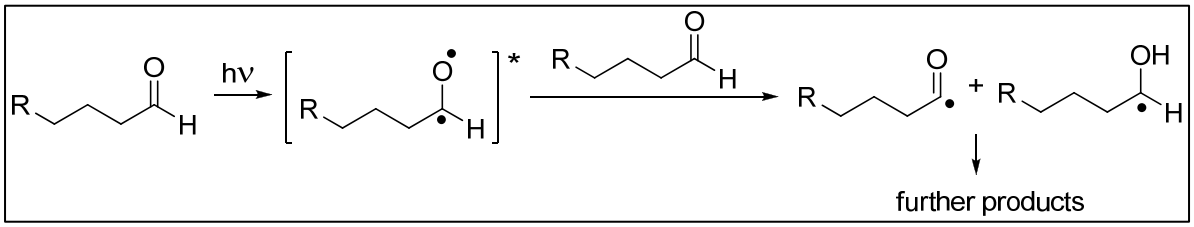

Figure 3.5 Autoinhibition Mechanism of Aldehydes. Adapted from Paquet et al[70].

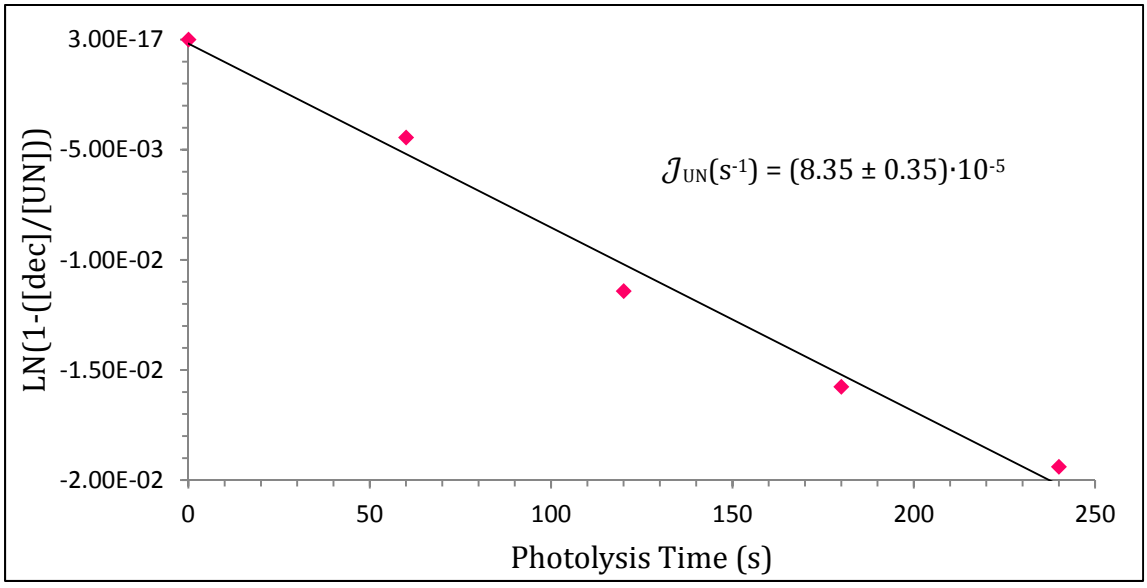

Figure 3.6 Formation of decane in undecanal photolysis.

FTIR data of liquid undecanal taken before photolysis is provided in Figure 3.7. The FTIR difference absorption spectra during photolysis are shown in Figure 3.8 and Figure 3.9. A few regions of the FTIR spectrum are oversaturated from the undecanal signal and differences are not mentioned for these regions. One can see the loss of undecanal by the decrease in the C-H stretch at 2818 cm^{-1}, Fermi resonance peak at 2714 cm^{-1}, C=O stretch at 1723 cm^{-1}, and some peaks in the fingerprint region. It is possible that an O-H stretch increases around 3,700-3,000 cm^{-1}, suggesting formation of products containing carboxyl groups. If an alcohol was produced, one would expect to see a C-O peak between 1,200-1,000 cm^{-1}, but there is none present. The growing peak at 3058 cm^{-1} can be attributed to a vinyl C-H stretch, either aliphatic (-$CH=CH_2$) or next to an oxygen atom (CH=CH-O). The former possibility would be consistent with the formation of 1-nonene, the expected Norrish Type II product of undecanal photolysis. A newly formed peak at 1710 cm^{-1} could be a C=O stretch of a carboxylic acid, ketone, or an α,β-unsaturated ester. An increase in peaks at 1220 cm^{-1} and 1265 cm^{-1} can be C-O stretches and/or C-H deformations of several types of compounds. In summary, the spectra are consistent with the formation of alkenes, carboxylic acids, ethers, and α,β-unsaturated esters as photolysis products.[74] Further analysis, in conjunction with GCMS measurements (in progress), is required to identify these products as many have common overlap with each other.

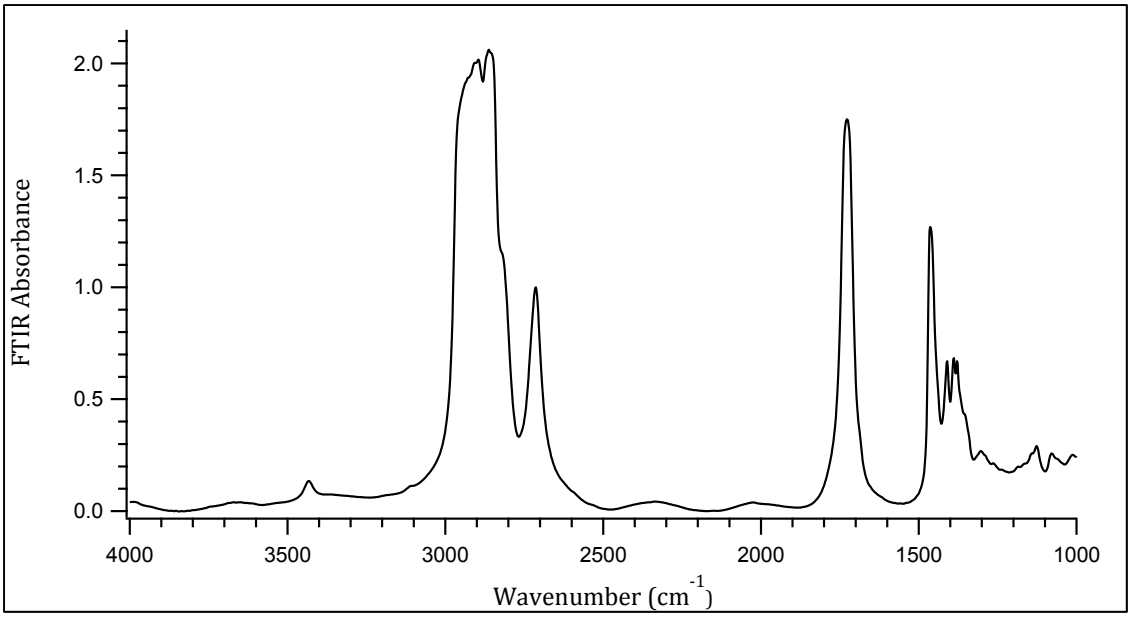

Figure 3.7 FTIR of undecanal

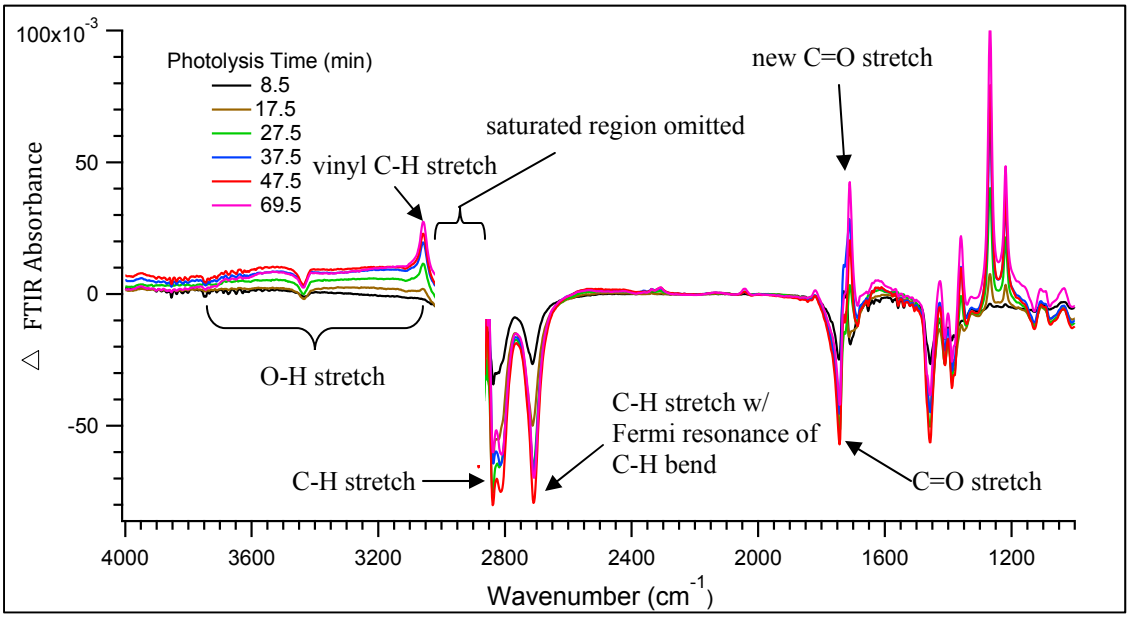

Figure 3.8 The change in FTIR absorbance during photolysis. The starting FTIR absorbance is subtracted from each FTIR absorbance during photolysis.

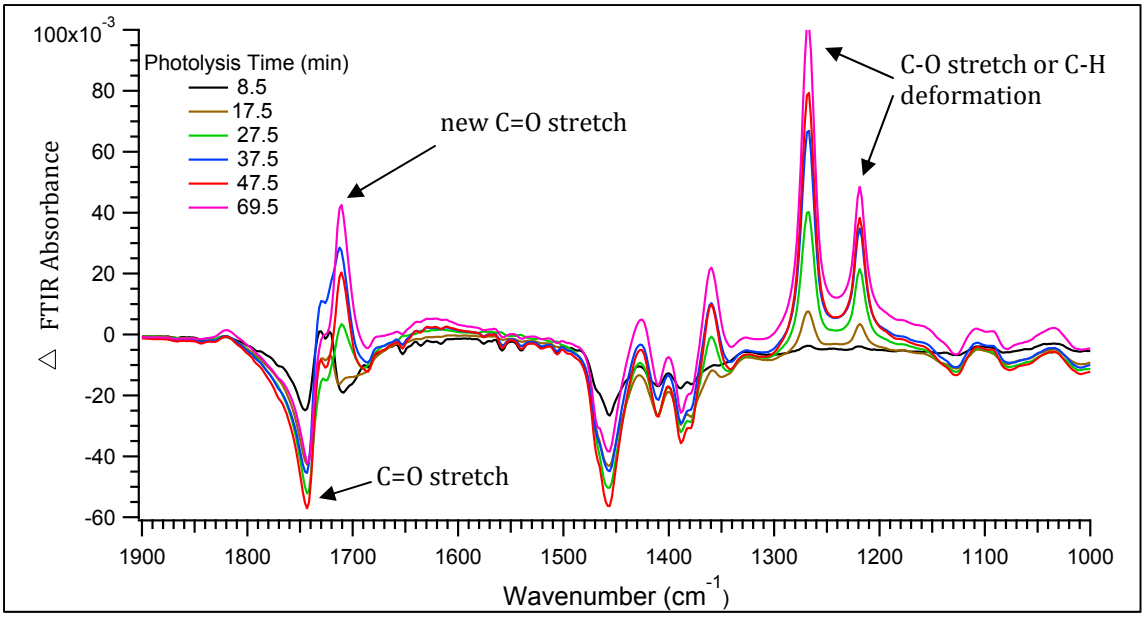

Figure 3.9 The change in FTIR absorbance during photolysis zoomed in.

CHAPTER 4: Summary and Future Experiments

The gas-phase quantum yield of undecanal (0.29 ± 0.11) is similar to those of other linear aliphatic aldehydes studied by Tadic et al[36]. Depending on the possible formation of undetected products, the liquid-phase quantum yield must be 0.18 ± 0.01 or greater. Aldehydes favor the Norrish Type I pathway versus ketones that produce more Norrish Type II products, and the expected decane product was formed.[53] FTIR experiments may be detecting some products that were not captured or collected during previous condensed-phase GCMS experiments; the formation of gas-phase products in addition to the previously observed decane product would result in an increase in the condensed-phase undecanal photolysis quantum yield. The condensed-phase photolysis of aldehydes is not significantly hindered relative to the gas-phase photolysis, suggesting that the photochemistry of aldehydes in SOA should be just as important as the photochemistry of gas-phase aldehydes. This hypothesis will be further tested with future experiments. These condensed-phase experiments will aim at monitoring the loss of the parent undecanal species for a more accurate total quantum yield and will look at temperature dependent trends. Also, the photochemistry between different phases in the atmosphere will be directly probed with SOA studies.

Future experiments include the previous experiments done in triplicate and studying a more thick and glassy phase of undecanal at temperatures below its the freezing point (-4 °C). The lower temperature and more structured form of undecanal will likely limit its photochemistry.[75] We aim to quantify this potential reduction in quantum yield and to determine the photolysis products. More atmospherically relevant studies will investigate

undecanal in SOA matrices. The mixture will be photolyzed in several different environments to understand the organic matrix type, phase, and temperature dependence of quantum yields and product composition. We will photolyze undecanal and SOA in aqueous solutions, organic solvents, and clean air, at or below room temperature. The samples will be monitored with FTIR, UV-vis, and HRMS. Reaction pathways, product characterization, and quantum yields of SOA under these conditions will provide insight to the photochemical aging of SOA in the atmosphere

REFERENCES

1. Sexton, K. G.; Jeffries, H. E.; Jang, M.; Kamens, R. M.; Doyle, M.; Voicu, I.; Jaspers, I., Photochemical Products in Urban Mixtures Enhance Inflammatory Responses in Lung Cells. *Inhalation Toxicol.* **2004,** *16* (Suppl. 1), 107-114.
2. U.S. EPA. Provisional Assessment of Recent Studies on Health Effects of Particulate Matter Exposure. U.S. Environmental Protection Agency, W., DC, EPA/600/R-12/056, 2012.
3. Mayoralas-Alises, S.; Diaz-Lobato, S., Air pollution and lung cancer. *Curr. Respir. Med. Rev.* **2012,** *8* (6), 418-429, 12 pp.
4. World Health Organization, Air Pollution Estimates. **2014**.
5. American Lung Association. "State of the Air 2014". **2014**.
6. Zhang, Q.; Jimenez, J. L.; Canagaratna, M. R.; Allan, J. D.; Coe, H.; Ulbrich, I.; Alfarra, M. R.; Takami, A.; Middlebrook, A. M.; Sun, Y. L.; Dzepina, K.; Dunlea, E.; Docherty, K.; DeCarlo, P. F.; Salcedo, D.; Onasch, T.; Jayne, J. T.; Miyoshi, T.; Shimono, A.; Hatakeyama, S.; Takegawa, N.; Kondo, Y.; Schneider, J.; Drewnick, F.; Borrmann, S.; Weimer, S.; Demerjian, K.; Williams, P.; Bower, K.; Bahreini, R.; Cottrell, L.; Griffin, R. J.; Rautiainen, J.; Sun, J. Y.; Zhang, Y. M.; Worsnop, D. R., Ubiquity and dominance of oxygenated species in organic aerosols in anthropogenically-influenced Northern Hemisphere midlatitudes. *Geophys. Res. Lett.* **2007,** *34* (13), L13801/1-L13801/6.
7. Kanakidou, M.; Seinfeld, J. H.; Pandis, S. N.; Barnes, I.; Dentener, F. J.; Facchini, M. C.; Van, D. R.; Ervens, B.; Nenes, A.; Nielsen, C. J.; Swietlicki, E.; Putaud, J. P.; Balkanski, Y.; Fuzzi, S.; Horth, J.; Moortgat, G. K.; Winterhalter, R.; Myhre, C. E. L.; Tsigaridis, K.; Vignati, E.; Stephanou, E. G.; Wilson, J., Organic aerosol and global climate modelling: A review. *Atmos. Chem. Phys.* **2005,** *5* (4), 1053-1123.
8. Putaud, J. P.; Van, D. R.; Alastuey, A.; Bauer, H.; Birmili, W.; Cyrys, J.; Flentje, H.; Fuzzi, S.; Gehrig, R.; Hansson, H. C.; Harrison, R. M.; Herrmann, H.; Hitzenberger, R.; Hueglin, C.; Jones, A. M.; Kasper-Giebl, A.; Kiss, G.; Kousa, A.; Kuhlbusch, T. A. J.; Loeschau, G.; Maenhaut, W.; Molnar, A.; Moreno, T.; Pekkanen, J.; Perrino, C.; Pitz, M.; Puxbaum, H.; Querol, X.; Rodriguez, S.; Salma, I.; Schwarz, J.; Smolik, J.; Schneider, J.; Spindler, G.; ten, B. H.; Tursic, J.; Viana, M.; Wiedensohler, A.; Raes, F., A European aerosol phenomenology - 3: Physical and chemical characteristics of particulate matter from 60 rural, urban, and kerbside sites across Europe. *Atmos. Environ.* **2010,** *44* (10), 1308-1320.
9. Minguillon, M. C.; Querol, X.; Baltensperger, U.; Prevot, A. S. H., Fine and coarse PM composition and sources in rural and urban sites in Switzerland: Local or regional pollution? *Sci. Total Environ.* **2012,** *427-428*, 191-202.
10. Donahue, N. M.; Henry, K. M.; Mentel, T. F.; Kiendler-Scharr, A.; Spindler, C.; Bohn, B.; Brauers, T.; Dorn, H. P.; Fuchs, H.; Tillmann, R.; Wahner, A.; Saathoff, H.; Naumann, K.-H.; Mohler, O.; Leisner, T.; Muller, L.; Reinnig, M.-C.; Hoffmann, T.; Salo, K.; Hallquist, M.; Frosch, M.; Bilde, M.; Tritscher, T.; Barmet, P.; Praplan, A. P.; DeCarlo, P. F.; Dommen, J.; Prevot, A. S. H.; Baltensperger, U., Aging of biogenic secondary organic aerosol via gas-phase OH radical reactions. *Proc. Natl. Acad. Sci. U. S. A., Early Ed.* **2012,** (Aug. 6 2012), 1-6, 6 pp.
11. Qi, L.; Nakao, S.; Cocker, D. R., Aging of secondary organic aerosol from Î±-pinene ozonolysis: Roles of hydroxyl and nitrate radicals. *J. Air Waste Manage. Assoc.* **2012,** *62* (12), 1359-1369.
12. Amin, H. S.; Hatfield, M. L.; Huff, H. K. E., Characterization of secondary organic aerosol generated from ozonolysis of Î±-pinene mixtures. *Atmos. Environ.* **2013,** *67*, 323-330.
13. Kalberer, M.; Paulsen, D.; Sax, M.; Steinbacher, M.; Dommen, J.; Prevot, A. S. H.; Fisseha, R.; Weingartner, E.; Frankevich, V.; Zenobi, R.; Baltensperger, U., Identification of Polymers as Major Components of Atmospheric Organic Aerosols. *Science (Washington, DC, U. S.)* **2004,** *303* (5664), 1659-1662.
14. Matsunaga, A.; Docherty, K. S.; Lim, Y. B.; Ziemann, P. J., Composition and yields of secondary organic aerosol formed from OH radical-initiated reactions of linear alkenes in the presence of NOx: Modeling and measurements. *Atmos. Environ.* **2009,** *43* (6), 1349-1357.
15. Lim, Y. B.; Ziemann, P. J., Chemistry of Secondary Organic Aerosol Formation from OH Radical-Initiated Reactions of Linear, Branched, and Cyclic Alkanes in the Presence of NOx. *Aerosol Sci. Technol.* **2009,** *43* (6), 604-619.

16. Pan, X.; Underwood, J. S.; Xing, J. H.; Mang, S. A.; Nizkorodov, S. A., Photodegradation of secondary organic aerosol generated from limonene oxidation by ozone studied with chemical ionization mass spectrometry. *Atmos. Chem. Phys.* **2009,** *9* (12), 3851-3865.
17. Shiraiwa, M.; Selzle, K.; Poeschl, U., Hazardous components and health effects of atmospheric aerosol particles: reactive oxygen species, soot, polycyclic aromatic compounds and allergenic proteins. *Free Radical Res.* **2012,** *46* (8), 927-939.
18. Takahama, S.; Schwartz, R. E.; Russell, L. M.; MacDonald, A. M.; Sharma, S.; Leaitch, W. R., Organic functional groups in aerosol particles from burning and non-burning forest emissions at a high-elevation mountain site. *Atmos. Chem. Phys.* **2011,** *11* (13), 6367-6386.
19. Schwartz, R. E.; Russell, L. M.; Sjostedt, S. J.; Vlasenko, A.; Slowik, J. G.; Abbatt, J. P. D.; MacDonald, A. M.; Li, S. M.; Liggio, J.; Toom-Sauntry, D.; Leaitch, W. R., Biogenic oxidized organic functional groups in aerosol particles from a mountain forest site and their similarities to laboratory chamber products. *Atmos. Chem. Phys.* **2010,** *10* (11), 5075-5088.
20. Gilardoni, S.; Russell, L. M.; Sorooshian, A.; Flagan, R. C.; Seinfeld, J. H.; Bates, T. S.; Quinn, P. K.; Allan, J. D.; Williams, B.; Goldstein, A. H.; Onasch, T. B.; Worsnop, D. R., Regional variation of organic functional groups in aerosol particles on four U.S. east coast platforms during the International Consortium for Atmospheric Research on Transport and Transformation 2004 campaign. *J. Geophys. Res., [Atmos.]* **2007,** *112* (D10), D10S27/1-D10S27/11.
21. Russell, L. M.; Bahadur, R.; Hawkins, L. N.; Allan, J.; Baumgardner, D.; Quinn, P. K.; Bates, T. S., Organic aerosol characterization by complementary measurements of chemical bonds and molecular fragments. *Atmos. Environ.* **2009,** *43* (38), 6100-6105.
22. Mang, S. A.; Henricksen, D. K.; Bateman, A. P.; Andersen, M. P. S.; Blake, D. R.; Nizkorodov, S. A., Contribution of Carbonyl Photochemistry to Aging of Atmospheric Secondary Organic Aerosol. *J. Phys. Chem. A* **2008,** *112* (36), 8337-8344.
23. Norrish, R. G. W.; Bamford, C. H., Photodecomposition of aldehydes and ketones. *Nature (London, U. K.)* **1936,** *138*, 1016.
24. Yang, N. C.; Yang, D.-D. H., Photochemical reactions of ketones in solution. *J. Am. Chem. Soc.* **1958,** *80*, 2913-14.
25. Sander, S. P., J. Abbatt, J. R. Barker, J. B. Burkholder, R. R. Friedl, D. M. Golden, R. E. Huie, C. E. Kolb, M. J. Kurylo, G. K. Moortgat, V. L. Orkin and P. H. Wine, "Chemical Kinetics and Photochemical Data for Use in Atmospheric Studies, Evaluation No. 17", JPL Publication 10-6, Jet Propulsion Laboratory, Pasadena, 2011 http://jpldataeval.jpl.nasa.gov.
26. Hallquist, M.; Wenger, J. C.; Baltensperger, U.; Rudich, Y.; Simpson, D.; Claeys, M.; Dommen, J.; Donahue, N. M.; George, C.; Goldstein, A. H.; Hamilton, J. F.; Herrmann, H.; Hoffmann, T.; Iinuma, Y.; Jang, M.; Jenkin, M. E.; Jimenez, J. L.; Kiendler-Scharr, A.; Maenhaut, W.; McFiggans, G.; Mentel, T. F.; Monod, A.; Prevot, A. S. H.; Seinfeld, J. H.; Surratt, J. D.; Szmigielski, R.; Wildt, J., The formation, properties and impact of secondary organic aerosol: current and emerging issues. *Atmos. Chem. Phys.* **2009,** *9* (14/2), 5155-5236.
27. Henry, K. M.; Donahue, N. M., Photochemical Aging of Î±-Pinene Secondary Organic Aerosol: Effects of OH Radical Sources and Photolysis. *J. Phys. Chem. A* **2012,** *116* (24), 5932-5940.
28. Bateman, A. P.; Nizkorodov, S. A.; Laskin, J.; Laskin, A., Photolytic processing of secondary organic aerosols dissolved in cloud droplets. *Physical Chemistry Chemical Physics* **2011,** *13* (26), 12199-12212.
29. Lignell, H.; Epstein, S. A.; Marvin, M. R.; Shemesh, D.; Gerber, B.; Nizkorodov, S., Experimental and Theoretical Study of Aqueous cis-Pinonic Acid Photolysis. *The Journal of Physical Chemistry A* **2013,** *117* (48), 12930-12945.
30. Calvert, J. G.; Pitts, J. N., *Photochemistry*. Wiley: New York, 1966.
31. Lee, E. K. C.; Lewis, R. S., Photochemistry of simple aldehydes and ketones in the gas phase. *Adv. Photochem.* **1980,** *12*, 1-96.
32. Warneck, P.; Moortgat, G. K., Quantum yields and photodissociation coefficients of acetaldehyde in the troposphere. *Atmos. Environ.* **2012,** *62*, 153-163.
33. Dorigo, A. E.; McCarrick, M. A.; Loncharich, R. J.; Houk, K. N., Transition structures for hydrogen atom transfers to oxygen. Comparisons of intermolecular and intramolecular processes, and open- and closed-shell systems. *J. Am. Chem. Soc.* **1990,** *112* (21), 7508-14.
34. Wagner, P. J.; Kelso, P. A.; Kemppainen, A. E.; Zepp, R. G., Type II photoprocesses of phenyl ketones. Competitive Î´-hydrogen abstraction and the geometry of intramolecular hydrogen atom transfers. *J. Amer. Chem. Soc.* **1972,** *94* (21), 7500-6.

35. McMillan, G. R.; Calvert, J. G.; Pitts, J. N., Jr., Detection and lifetime of enol-acetone in the photolysis of 2-pentanone vapor. *J. Am. Chem. Soc.* **1964,** *86* (18), 3602-5.
36. Tadic, J. M.; Xu, L.; Houk, K. N.; Moortgat, G. K., Photooxidation of n-octanal in air: experimental and theoretical study. *J. Org. Chem.* **2011,** *76* (6), 1614-1620.
37. Zhu, L.; Tang, Y.; Chen, Y.; Cronin, T., Wavelength-Dependent Photolysis of C3-C7 Aldehydes in the 280-330 nm Region. *Spectrosc. Lett.* **2009,** *42* (8), 467-478.
38. Horspool, W.; Lenci, F., *CRC Handbook of Organic Photochemistry and Photobiology: Second Edition*. CRC Press LLC: 2004.
39. Reichardt, C. W., T., Solvents and Solvent Effects in Organic Chemistry. Wiley-VCH Verlag GmbH & Co. KGaA: 2011.
40. Neuman, R. C., Pressure effects as mechanistic probes of organic radical reactions. *Accounts of Chemical Research* **1972,** *5* (11), 381-387.
41. Tatum, E. C.; Bauer, D.; Hynes, A. J., Radical Quantum Yields from Formaldehyde Photolysis in the 30 400-32 890 cm-1 (304-329 nm) Spectral Region: Detection of Radical Photoproducts Using Pulsed Laser Photolysis-Pulsed Laser Induced Fluorescence. *J. Phys. Chem. A* **2012,** *116* (26), 6983-6995.
42. Hung, K.-C.; Tsai, P.-Y.; Li, H.-K.; Lin, K.-C., Photodissociation of CH3CHO at 248 nm by time-resolved Fourier-transform infrared emission spectroscopy: Verification of roaming and triple fragmentation. *J. Chem. Phys.* **2014,** *140* (6), 064313/1-064313/11.
43. Chen, Y.; Zhu, L., The Wavelength Dependence of the Photodissociation of Propionaldehyde in the 280-330 nm Region. *J. Phys. Chem. A* **2001,** *105* (42), 9689-9696.
44. Jimenez, E.; Lanza, B.; Martinez, E.; Albaladejo, J., Daytime tropospheric loss of hexanal and trans-2-hexenal: OH kinetics and UV photolysis. *Atmos. Chem. Phys.* **2007,** *7* (6), 1565-1574.
45. Tadic, J. M.; Moortgat, G. K.; Bera, P. P.; Loewenstein, M.; Yates, E. L.; Lee, T. J., Photochemistry and Photophysics of n-Butanal, 3-Methylbutanal, and 3,3-Dimethylbutanal: Experimental and Theoretical Study. *J. Phys. Chem. A* **2012,** *116* (24), 5830-5839.
46. Tadic, J.; Juranic, I.; Moortgat, G. K., Pressure dependence of the photooxidation of selected carbonyl compounds in air: n-butanal and n-pentanal. *J. Photochem. Photobiol., A* **2001,** *143* (2-3), 169-179.
47. Tadic, J.; Juranic, I.; Moortgat, G. K., Photooxidation of n-hexanal in air. *Molecules* **2001,** *6* (4), 287-299.
48. Paulson, S. E.; Liu, D.-L.; Orzechowska, G. E.; Campos, L. M.; Houk, K. N., Photolysis of Heptanal. *J. Org. Chem.* **2006,** *71* (17), 6403-6408.
49. Zhang, J.; Zhang, P., Study on photochemical degradation of nonanal-an odorant in gas phase by vacuum ultraviolet. *Huanjing Gongcheng Xuebao* **2010,** *4* (6), 1368-1372.
50. Lebourgeois, P.; Arnaud, R.; Lemaire, J., Population of triplet state nÎ * of saturated aliphatic aldehydes. *J. Chim. Phys. Phys.-Chim. Biol.* **1976,** *73* (2), 135-40.
51. Ervens, B.; Wang, Y.; Eagar, J.; Leaitch, W. R.; Macdonald, A. M.; Valsaraj, K. T.; Herckes, P., Dissolved organic carbon (DOC) and select aldehydes in cloud and fog water: the role of the aqueous phase in impacting trace gas budgets. *Atmos. Chem. Phys.* **2013,** *13* (10), 5117-5135, 19 pp.
52. Bamford, C. H.; Norrrish, R. G. W., Primary photochemical reactions. XI. The photolysis of aldehydes and ketones in paraffinoid solution. *J. Chem. Soc.* **1938**, 1531-43.
53. Gugumus, F., Contribution to the role of aldehydes and peracids in polyolefin oxidation 1. Photolysis and photooxidation of aldehydes in polyethylene. *Polym. Degrad. Stab.* **1999,** *65* (2), 259-269.
54. Appel, W. K.; Jiang, Z. Q.; Scheffer, J. R.; Walsh, L., Crystal lattice control of unimolecular photorearrangements. Medium-dependent photochemistry of cyclohexenones. *Journal of the American Chemical Society* **1983,** *105* (16), 5354-5363.
55. Jenkins, C. A.; Murphy, D. M., Thermal and Photoreactivity of TiO2 at the Gas-Solid Interface with Aliphatic and Aromatic Aldehydes. *J. Phys. Chem. B* **1999,** *103* (6), 1019-1026.
56. Hunter, E. P. L.; Lias, S. G., Evaluated Gas Phase Basicities and Proton Affinities of Molecules: An Update. *J. Phys. Chem. Ref. Data* **1998,** *27* (3), 413-656.
57. Keller-Rudek, H., Moortgat, G. K., Sander, R., and Sörensen, R., The MPI-Mainz UV/VIS spectral atlas of gaseous molecules of atmospheric interest. *Earth Syst. Sci. Data* **2013,** *5*, 365–373.
58. International Programme on Chemical Safety.Environmental Health Criteria 164. Methylene Chloride.Second Edition.Geneva:World Health Organization. 1996.
59. Donten, M. L.; Hamm, P.; Vande, V. J., A Consistent Picture of the Proton Release Mechanism of oNBA in Water by Ultrafast Spectroscopy and Ab Initio Molecular Dynamics. *J. Phys. Chem. B* **2011,** *115* (5), 1075-1083.

60. Galbavy, E. S.; Ram, K.; Anastasio, C., 2-Nitrobenzaldehyde as a chemical actinometer for solution and ice photochemistry. *J. Photochem. Photobiol., A* **2010,** *209* (2-3), 186-192.
61. Willett, K. L.; Hites, R. A., Chemical actinometry: using o-nitrobenzaldehyde to measure light intensity in photochemical experiments. *J. Chem. Educ.* **2000,** *77* (7), 900-902.
62. Pitts, J. N., Jr.; Wan, J. K. S.; Schuck, E. A., Photochemical studies in an alkali halide matrix. I. An o-nitrobenzaldehyde actinometer and its application to a kinetic study of the photoreduction of benzophenone by benzhydrol in a pressed potassium bromide disk. *J. Am. Chem. Soc.* **1964,** *86* (18), 3606-10.
63. Diskin, A. M.; Wang, T.; Smith, D.; Spanel, P., A selected ion flow tube (SIFT), study of the reactions of H3O+, NO+ and O2+ ions with a series of alkenes; in support of SIFT-MS. *Int. J. Mass Spectrom.* **2002,** *218* (1), 87-101.
64. Buhr, K.; van Ruth, S.; Delahunty, C., Analysis of volatile flavor compounds by Proton Transfer Reaction-Mass Spectrometry: fragmentation patterns and discrimination between isobaric and isomeric compounds. *Int. J. Mass Spectrom.* **2002,** *221* (1), 1-7.
65. Finlayson-Pitts, B. J. P. J. N., *Chemistry of the upper and lower atmosphere : theory, experiments, and applications*. Academic Press: San Diego, 2000.
66. Osif, T. L.; Heicklen, J., Oxidation of formyl radicals. *The Journal of Physical Chemistry* **1976,** *80* (14), 1526-1531.
67. Tso, T. L.; Diem, M.; Lee, E. K. C., Oxidation of formyl radical in solid molecular oxygen at 13 K: formation of formic acid and formylperoxy radical, HC(O)OO. *Chem. Phys. Lett.* **1982,** *91* (5), 339-42.
68. WrÃ³blewski, T.; Ziemczonek, L.; Szerement, K.; Karwasz, G. P., Proton affinities of simple organic compounds. *Czechoslovak Journal of Physics* **2006,** *56* (2), B1110-B1115.
69. Kossanyi, J.; Sabbah, S.; Chaquin, P., Photochemistry in solution. XX. Triplet reactivity of aliphatic aldehydes. *Tetrahedron* **1981,** *37* (19), 3307-15.
70. Paquet, P.; Fellous, R.; Stringat, R.; Fabre, G., Pulsed-laser photochemistry of pentanal at 355 nm. *Tetrahedron Lett.* **1992,** *33* (4), 485-6.
71. Fujisawa, T.; Monroe, B. M.; Hammond, G. S., Rates of termination of radicals in solution. V. Ketyl radicals derived from Î±-oxo acids and esters. *J. Amer. Chem. Soc.* **1970,** *92* (3), 542-4.
72. Schuster, D. I.; Karp, P. B., Photochemistry of ketones in solution. LVIII: Mechanism of photoreduction of benzophenone by benzhydrol. *J. Photochem.* **1980,** *12* (4), 333-44.
73. Funke, C. W.; Cerfontain, H., Photoreduction of cycloalkanecarbaldehydes. *J. Chem. Soc., Perkin Trans. 2* **1976,** (6), 669-73.
74. Socrates, G. S. G., *Infrared and Raman characteristic group frequencies : tables and charts*. Wiley: Chichester; New York, 2000.
75. Klan, P.; Janosek, J.; Kriz, Z., Photochemistry of valerophenone in solid solutions. *J. Photochem. Photobiol., A* **2000,** *134* (1-2), 37-44.

APPENDIX: Photolysis Calculations

Rate Equation for Photolysis:

$$R = \frac{f_{irradiated}}{b} \cdot \int_{\lambda_1}^{\lambda_2} D_o(\lambda)\left[1 - e^{-\sigma(\lambda)\cdot n\cdot b}\right] \cdot \phi(\lambda) d\lambda$$

$$\alpha = \frac{R_o \cdot b}{f_{irradiated} \cdot \langle\phi\rangle \cdot \int_{\lambda_1}^{\lambda_2} OO(\lambda) \cdot [1 - e^{-\sigma(\lambda)\cdot n\cdot b}] d\lambda}$$

$$\langle\phi\rangle = \frac{R_o \cdot b}{f_{irradiated} \cdot \int_{\lambda_1}^{\lambda_2} D_o(\lambda) \cdot [1 - e^{-\sigma(\lambda)\cdot n\cdot b}] d\lambda}$$

Simplified equations for small absorption limit for gas-phase:

$$R = f_{irradiated} \cdot n \cdot \int_{\lambda_1}^{\lambda_2} D_o(\lambda) \cdot \sigma(\lambda) \cdot \phi(\lambda) d\lambda$$

$$\mathcal{J} = f_{irradiated} \cdot \int_{\lambda_1}^{\lambda_2} D_o(\lambda) \cdot \sigma(\lambda) \cdot \phi(\lambda) d\lambda$$

$$\alpha = \frac{\mathcal{J}}{f_{irradiated} \cdot \langle\phi\rangle \int_{\lambda_1}^{\lambda_2} OO(\lambda) \cdot \sigma(\lambda) d\lambda}$$

$$\langle\phi\rangle = \frac{\mathcal{J}}{f_{irradiated} \cdot \int_{\lambda_1}^{\lambda_2} D_o(\lambda) \cdot \sigma(\lambda) d\lambda}$$

Where

$$D_o(\lambda) = \alpha \cdot OO(\lambda)$$